Nano-TiO₂ Reinforced PEEK/PEI Blends as Biomaterials for Load-Bearing Implant Applications

Ana M. Díez-Pascual*,[†] and Angel L. Díez-Vicente[‡]

[†]Analytical Chemistry, Physical Chemistry and Chemical Engineering Department, Faculty of Biology, Environmental Sciences and Chemistry, Alcalá University, Alcalá de Henares, Madrid E-28871, Spain

[‡]Airbus Operations S. L., John Lennon s/n, Getafe, Madrid 28906, Spain

ABSTRACT: Biocompatible ternary nanocomposites based on poly(ether ether ketone) (PEEK)/poly(ether imide) (PEI) blends reinforced with bioactive titanium dioxide (TiO₂) nanoparticles were fabricated via ultrasonication followed by melt-blending. The developed biomaterials were characterized using FT-IR, SEM, XRD, DSC, TGA, and DMA. Further, their water-absorption, tensile, tribological, dielectric, and antibacterial properties were evaluated. PEI acts as a coupling agent, since it can interact both with PEEK via π–π stacking and polar interactions as well as with the nanoparticles through hydrogen bonding, as corroborated by the FT-IR spectra, which resulted in a homogeneous titania dispersion within the biopolymer blend without applying any particle surface treatment or polymer functionalization. A change from promotion to retardation in the crystallization rate of the matrix was found with increasing TiO₂ concentration, while its crystalline structure remained unaltered. The nanoparticles stiffened, strengthened, and toughened the matrix simultaneously, and the optimal properties were achieved at 4.0 wt % TiO₂. More interesting, the tensile properties were retained after steam sterilization in an autoclave or exposure to a simulated body fluid (SBF). The nanocomposites also displayed reduced water absorption though higher thermal stability, storage modulus, glass transition temperature, dielectric constant, and dielectric loss compared to the control blend. Further, remarkable enhancements in the tribological properties under both SBF and dry environments were attained. The nanoparticles conferred antibacterial action versus Gram-positive and Gram-negative bacteria in the presence and the absence of UV light, and the highest inhibition was attained at 4.0 wt % nanoparticle concentration. These nanocomposites are expected to be used in long-term load-bearing implant applications.

KEYWORDS: PEEK/PEI blends, biocomposites, TiO₂ nanoparticles, antimicrobials, load-bearing implants
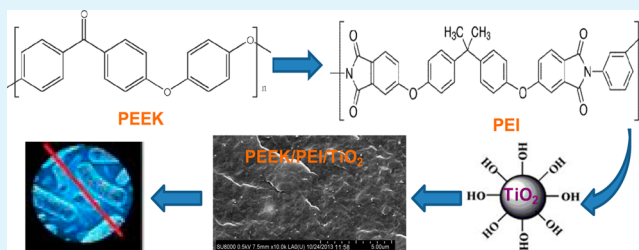
1. INTRODUCTION

Recently, there is a strong request for materials that imitate living tissues for the sake of physicomechanical, biological, and functional properties. Conventionally, metals or ceramics were selected for hard tissue applications. In particular, titanium alloys were broadly used over the past decades for implantable devices such as orthopedic implants and artificial blood vessels due to their low density, outstanding corrosion resistance, excellent mechanical performance, cytocompatibility, and ability to adhere to bone and other tissues (osseointegration).[1] However, their high cost, the divergence between the mechanical performance of Ti alloys and human bones, and the worries about adverse reactions after implantation have lately limited their use, and substitutes are required.[2] In this regard, polymeric materials offer a wide variety of properties. Polyurethane (PU), ultrahigh molecular weight polyethylene (UHMWPE), polyoxymethylene (POM), and poly(ether ether ketone) (PEEK) are thermoplastics frequently used in the fabrication of in vivo devices.[3] PEEK biomaterial has been increasingly employed for orthopedic, trauma, spinal, and dental implants[4] due to its biocompatibility and in vivo stability. From an engineering standpoint, its properties such as superior stiffness, strength, toughness, excellent thermal stability, outstanding creep performance, resistance to chemical and radiation damage together with its bioactivity and non-cytotoxicity, make it a multipurpose biomaterial greatly suitable for the development of medical device applications.[5] In addition, it is translucent to X-rays, insulating, and nonmagnetic and can be repeatedly sterilized using γ radiation, ethylene oxide gas, and steam without modifying its mechanical properties or biocompatibility. PEEK is being investigated in practically all application areas for long-term implants, including finger joints, spinal cages, bone replacements, screws and pins for bone fixation, as well as dental crowns and posts.[4]

The characteristics of implantable-grade PEEK must be tailored to match specific tissue properties. For instance, to simulate the longitudinal elastic modulus of human cortical bone (14−20 GPa), the mechanical performance of this thermoplastic can be additionally improved by incorporating particles or fibers. Thus, the addition of 30 wt % short carbon

fibers (SCF) to the base polymer can raise the stiffness from ∼4 to 18 GPa and the strength from 100 to 230 GPa.[6] However, when SCF-reinforced PEEK was used in tibial and acetabular components, some of them failed due to debonding of the SCFs under high loads. To enhance implant fixation, bioactive materials such as hydroxyapatite (HA)[7,8] have been incorporated into this polymer, although the mechanical performance of the resulting composites was poor due to weak PEEK–HA bonding. Consequently, a lot of interest has recently been generated in manufacturing nanoparticle-reinforced PEEK composites owing to the exceptional properties originating from their nanoscale structure.[9] The nanoparticles possess very high surface-to-volume ratio, and hence can lead to a large interface, which results in strong filler–matrix interfacial adhesion. Concerning this, different inorganic nanoparticles like silica (SiO_2),[10] metal oxides (Al_2O_3, ZnO),[11,12] silicon carbide (SiC),[13] silicon nitride (Si_3N_4),[14] and transition metal chalcogenides (WS_2)[15,16] have been incorporated in PEEK, albeit with only moderate success. Thus, a uniform dispersion of the nanoreinforcements within the matrix is essential for improving the mechanical performance.[9] However, this is a very difficult chore in the case of PEEK nanocomposites since they cannot be processed through solution methods due to the insolubility of this thermoplastic in most solvents apart from concentrated hydrofluoric and methanesulfonic acids,[9] which results in extremely high melt viscosity, together with the strong agglomerating tendency of the nanoparticles. Thus, visible aggregates are generally found for nanoparticle loadings ≥2.5 wt %. In addition, some of these nanoparticles are expensive, which is reflected in a rise in composite price.

An alternative strategy is the blending with other biopolymers, a cheaper route that enables to obtain high-performance biomaterials that combine the complementary properties of both constituents. This is particularly attractive in blends with poly(ether imide) (PEI),[17] a biocompatible amorphous thermoplastic structurally similar to and miscible with PEEK. PEI presents excellent properties even at elevated temperature, namely, high chemical inertness and resistance to all sterilization techniques,[17−19] and it is currently used in a large number of electronic and medical applications including surgical devices and dental and orthopedic tools. Over the past years, several articles dealing with the morphological, thermal, and mechanical characterization of PEEK/PEI blends have been published.[20−22] Interestingly, the mixtures displayed a maximum in ductility and toughness at intermediate compositions (20−30 wt % PEI) that coincided with a maximum in PEEK crystallinity. Blends are preferred over PEEK since they are considerably cheaper, tougher, maintain rigidity at higher temperatures due to their higher T_g, and display enhanced thermal stability and high heat distortion temperature.

Over recent years, a lot of effort has been devoted to the research of titanium dioxide (titania, TiO_2) nanostructures due to their extraordinary optical, electrical, and photocatalytic properties. They are inert, safe, reasonably priced, and environmentally friendly inorganic n-type semiconductors that display superior mechanical properties, intense UV absorption, low coefficient of thermal expansion, elevated thermal conductivity, superior hydrophilicity, and strong antibacterial action versus a broad range of microorganisms.[23] The antibacterial characteristics of irradiated TiO_2 materials have been reported to originate from the combined action of their self-cleaning and self-disinfection properties,[24] though the

detailed mechanism that causes bacterial cell death is not clear yet. It has been reported that TiO_2 nanoparticles have higher bioactivity than conventional microparticles.[25] In particular, osteoblasts and chondrocytes exhibit an expanded morphology and increased proliferation when exposed to TiO_2 nanofillers compared with cells exposed to micron-sized particles. Further, the strength of bone–titanium integration is considerably greater for implants with nanoparticles. In this regard, a few nano-TiO_2 reinforced biopolymers such as poly-L-lactide (PLLA),[26] poly(lactic-co-glycolic acid) (PLGA),[27] and poly(phenylsulfone) (PPSU)[28] have been developed for biomaterial applications. Nevertheless, TiO_2 nanoparticles are not regularly employed so far as antibacterial materials in medical implants or devices.[28]

The present study reports the synthesis of nano-TiO_2 reinforced PEEK/PEI blends via ultrasonication followed by melt-blending, a common and versatile method easy to scale up. A comprehensive characterization was performed to evaluate in detail the influence of the nanoparticles on the morphology, crystallization behavior, thermal stability, static and dynamic mechanical performance, tribological, dielectric, and antibacterial properties of these new biomaterials that are very promising for use in medical implant applications.

2. EXPERIMENTAL SECTION

Materials. Zeniva poly(ether ether ketone), PEEK $(d_{25 °C} = 1.30$ g/cm^3, $T_g \approx 147$ °C, $T_m \approx 343$ °C), was supplied by Solvay Specialty Polymers. ULTEM poly(ether imide), PEI $(d_{25 °C} = 1.27$ g/cm^3, $T_g \approx 217$ °C), was provided by Sabic Innovative Plastics. Their chemical structures are shown in Scheme 1. Both biopolymers are high-purity

Scheme 1. Chemical Structure of (a) Poly(ether ether ketone) (PEEK) and (b) Polyetherimide (PEI)
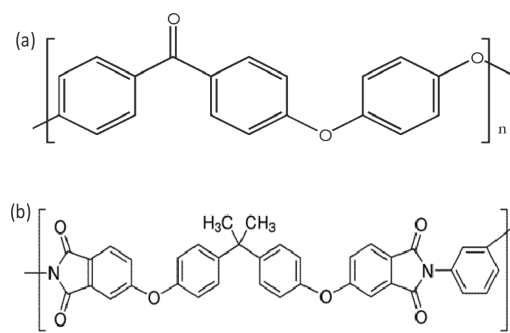
grades that satisfy USP Class VI and ISO 10993 criteria.[29] The polymers were vacuum-dried at 120 °C for 4 h and stored in a dry environment before blending. Titanium(IV) oxide nanopowder, TiO_2, was supplied by Sigma-Aldrich.[28]

Nanocomposite Preparation. To assess the optimal PEEK/PEI blend ratio for the preparation of the nanocomposites, five mixtures of compositions 90/10, 80/20, 70/30, 60/40, and 50/50 wt/wt % were initially prepared via extrusion at 380 °C in a Thermo-Haake MiniLab microextruder. Mixing times of 20 min and a rotor speed of 150 rpm were applied.[17] A PEEK/PEI blend with a ratio of 70/30 was chosen as matrix material due to its optimum balance between stiffness, toughness, thermal stability, and glass transition temperature. The nanocomposites were manufactured via ultrasonication and melt-blending, following a procedure similar to that reported previously.[29] First, PEEK and PEI (70/30 wt/wt %) were ball-milled to reduce their particle size. Second, the required amount of TiO_2 nanoparticles and the polymer powder were ultrasonicated in ethanol, vacuum-dried to remove the solvent, and subsequently melt-blended under the above-mentioned conditions. Four nanocomposites were manufactured, with

final TiO$_2$ concentrations of 1.0, 2.0, 4.0, and 8.0 wt %. The nanocomposites were then hot-pressed at 380 °C under 130 bar for 5 min and finally annealed.[29]

Characterization Techniques. The state of dispersion of the nanoparticles was characterized using an SU8000 Hitachi scanning electron microscope (SEM).[28] The attenuated total reflectance-Fourier transform infrared (ATR-FTIR) spectra were recorded on a PerkinElmer Spectrum One spectrometer.[12] The thermal stability of the composites was analyzed by thermogravimetric analysis (TGA) using a TA Instruments Q50 thermobalance.[16] Dynamic differential scanning calorimetry (DSC) experiments were conducted on a Mettler TA 400/DSC 30 differential scanning calorimeter. Samples were heated to 380 °C, cooled to 40 °C, and then reheated to 380 °C at a rate of 10 °C/min. The level of crystallinity (X_c) of the nanocomposites was estimated using a melt enthalpy of 100% crystalline PEEK equal to 130 J/g.[17] X-ray diffraction (XRD) measurements were carried out on a Bruker D8 Advance diffractometer using Cu Kα radation (λ = 1.54 Å).[28]

The water absorption was calculated based on the ASTM D570 standard. Samples were initially dried in an oven for one week, placed in a desiccator to cool, and then weighed. Subsequently, they were submerged in distilled water at 25 ± 2 °C. After certain time intervals, the samples were taken out, the water on the surface was completely eliminated using tissue paper, and the samples were weighed. Immediately, the samples were replaced into the water. The water absorption was calculated as $[(W_t - W_i)/W_i] \times 100$, where W_i and W_t are the initial dry mass and the instantaneous weight of the samples after exposure to water for different periods of time, respectively. Five determinations were performed for each sample to obtain an average value.

The dynamic mechanical properties of the composites were studied using a Mettler DMA 861 dynamic mechanical analyzer[30] in the temperature range between −130 and 260 °C. Tensile tests were performed at 23 °C and 50% relative humidity (RH) using an INSTRON 4204 mechanical tester according to the UNE-EN ISO 527−1 standard. Tensile measurements were also performed on samples subjected to 10 sterilization cycles in an autoclave at 124 °C and 2 bar, following the EN ISO 17665 standard, and on composites immersed in an SBF at 37 °C for 10 weeks.[28]

The room temperature dielectric properties were measured with an HP 4294 impedance analyzer in the frequency range between 10 and 1 × 10^6 Hz. Tribological properties were investigated with a pin-on-disc tribometer (MT/10/SCM from Microtest).[28] Experiments were performed at 23 °C and 10% RH and in SBF medium at 37 °C for a period of 6 h. Three replicate experiments were performed to check for repeatability and consistency of the assay.

The antibacterial activity of the nanocomposites was evaluated both in the presence and the absence of UV light against two test microorganisms: Gram-positive *Staphylococcus aureus* (*S. aureus*, ATCC 12600) and Gram-negative *Escherichia coli* (*E. coli*, ATCC 25922).[12] The survival ratio (SR) was estimated following the equation SR = $(N/N_o) \times 100$, where N_o and N are the average number of bacteria on the reference blend and the nanocomposites, respectively. Three tests were performed to obtain a mean value.

3. RESULTS AND DISCUSSION

SEM Analysis. As mentioned in the introduction, particle size and size distribution as well as level of dispersion play a key role on the composite performance. Consequently, SEM analysis was carried out to obtain information about the surface morphology of the nanocomposites, and representative images of the PEEK/PEI (70/30 wt/wt %) blend filled with 1.0 and 8.0 wt % TiO$_2$ are displayed in Figure 1. For all the nanocomposites, a single polymeric phase was detected, thereby confirming the complete miscibility of both thermoplastics, as previously reported.[21] The spherical white dots in the micrographs correspond to the anatase TiO$_2$ nanoparticles that exhibit a wide size distribution, with diameters in the range
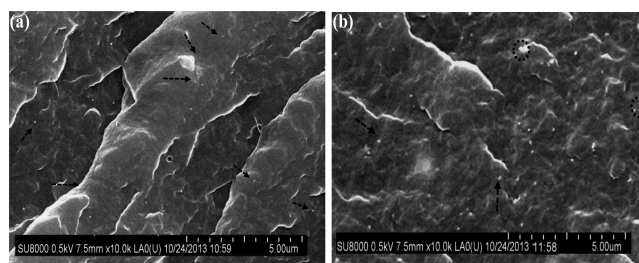

Figure 1. Typical SEM images of PEEK/PEI/TiO$_2$ nanocomposites with 1.0 wt % (a) and 8.0 wt % (b) nanoparticle loading. The arrows indicate TiO$_2$ nanoparticles randomly distributed within the matrix. The circles in (b) show small clusters of three or four nanoparticles.

of 40−120 nm and an average value of 75 nm. In both nanocomposites, the nanoparticles are randomly and homogeneously distributed within the matrix, and a uniform, aggregate-free nanofiller dispersion was found throughout the examined areas. Nonetheless, the dispersion is finer in the sample with the lowest TiO$_2$ loading (Figure 1a) that shows an average interparticle distance of ∼1 μm, whereas that with the highest concentration presents considerably reduced particle−particle distance, and even a few small clusters (240−380 nm size) comprising three or four particles can be visualized (Figure 1b). An analogous morphology with homogeneously dispersed nanofillers was also observed in the nanocomposites reinforced with 2.0 or 4.0 wt % TiO$_2$, which reveals that the preprocessing ultrasonication stage combined with the interactions between the polar groups of the matrix (imide, ketone, ether) and the OH moieties of the nanoparticles preclude TiO$_2$ agglomeration. In fact, PEI is acting as a coupling agent in the nanocomposites, since it can interact both with PEEK via π−π stacking and polar interactions as well as with the nanoparticles through formation of hydrogen bonds between the carbonyl groups of the imide rings and the hydroxyl moieties on the nanoparticle surface. Overall, SEM analysis demonstrates that the combination of ultrasonication and melt blending was certainly useful for homogeneously dispersing TiO$_2$ within the PEEK/PEI mixture at a nanoscale level without applying any particle surface treatment or polymer functionalization, making the fabrication of these biomaterials easy, fast, cost-effective, and suitable for large-extent production.

Fourier-Transform Infrared Study. To provide information about the polymer−polymer and nanoparticle−polymer interactions, the ATR-FTIR spectra of bare TiO$_2$ nanoparticles, neat PEEK, PEI, the binary PEEK/PEI (70/30 wt/wt %) sample, and the nanocomposites with 1.0 and 8.0 wt % TiO$_2$ concentration were recorded and are compared in Figure 2. The spectrum of TiO$_2$ exhibits an intense and wide band centered at ∼3400 cm^{-1} attributed to the O−H stretching, as well as peaks at 1630 and 1012 cm^{-1} arising from the bending vibration of coordinated H$_2$O and Ti−OH.[31] The peak at ∼650 cm^{-1} is related to the Ti−O−Ti stretching, and that at 1400 cm^{-1} has been assigned to TiO$_2$ lattice vibrations.[32] Pure PEEK displays a typical peak at 1650 cm^{-1} referred to the C=O stretching, and the peaks at 1595 and 1490 cm^{-1} correspond to the C−C stretching of the aromatic rings.[33] Further, the C−O−C stretching vibrations of the aromatic ether bond appear at 1220 and 1080 cm^{-1}, and the C−H wagging vibrations appear at 830 and 766 cm^{-1}.

On another note, the spectrum of neat PEI displays typical imide bands at 1780 and 1720 cm^{-1} arising from the carbonyl asymmetrical and symmetrical stretching vibrations, as well as
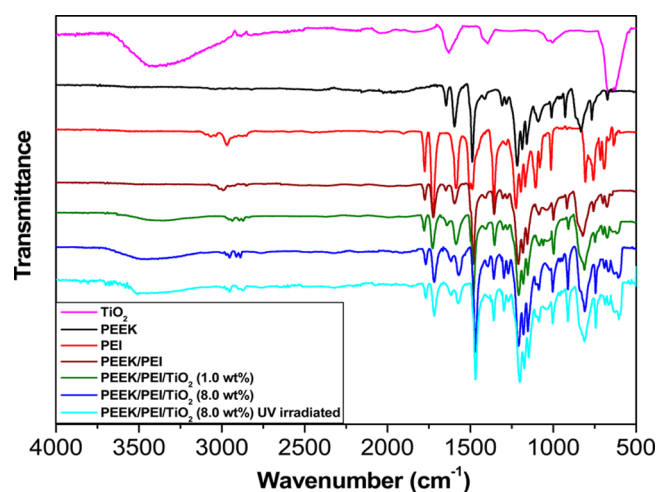
Figure 2. ATR-FTIR spectra of TiO_2, neat PEEK, PEI, PEEK/PEI (70/30 wt/wt %), and the nanocomposites with 1.0 and 8.0 wt % TiO_2 content. The spectrum of the nanocomposite with the highest nanoparticle concentration after UV irradiation is also plotted.

peaks at 1355 and 750 cm^{-1} associated with the C−N stretching and bending, respectively.[31] The sharp peak at 1588 cm^{-1} corresponds to the C−C stretching of the aromatic rings, and that at 1230 cm^{-1} is attributed to the C−O−C stretching of the ether group. Further, the C−H stretching vibrations of the methyl groups appear at 2970 and 2900 cm^{-1}. As expected, the spectrum of the binary PEEK/PEI blend exhibits the characteristic peaks of both polymers, their intensities being consistent with the blend composition. Interestingly, the C−C stretching vibrations of the aromatic rings are shifted toward lower wavenumbers, as well as the C−H wagging. The red shift of these bands has been ascribed to intense π−π stacking interactions between compounds with aromatic rings,[34] corroborating that the aromatic moieties of both biopolymers strongly interact via π−π stacking.

The spectra of the nanocomposites are similar to that of the polymer blend, with a few peaks characteristic of TiO_2. A broadening an upshift of the band referred to the O−H stretching is detected compared to that of the raw nanoparticles, by ∼10 and 35 cm^{-1} for the composites with 1.0 and 8.0 wt % TiO_2, respectively. Such phenomenon points toward H-bond formation with the ketone group of PEEK at the cost of disrupting the H-bonds among OH moieties of the nanoparticles.[28] More significantly, the band referred to as the C=O stretching is broader and appears at lower wavenumbers in comparison to that of pure PEEK, the downshift being 12 and 36 cm^{-1} for the nanocomposites with 1.0 and 8.0 wt % TiO_2, respectively, also indicative of H-bond formation with the OH moieties of TiO_2. Moreover, the wide peak related to the Ti−O−Ti stretching moves down to 632 and 618 cm^{-1} in the two aforementioned nanocomposites, yet one more evidence of the existence of nanoparticle−polymer interactions, these effects exacerbating with increasing TiO_2 loading. As expected, this band is stronger in the nanocomposite with 8.0 wt % in comparison to that with 1.0 wt %, consistent with its higher nanoparticle concentration.

To assess the stability of the developed nanocomposites under UV light irradiation, the spectrum of PEEK/PEI/TiO_2 (8.0 wt %) was recorded after illumination with 365 nm UV light for 24 h, and it is also plotted in Figure 2 for comparison. The photocatalytic degradation of PEEK causes random

homolytic chain scission reactions, cross-linking, and formation of carbonyl and hydroxyl groups.[35] Thus, if the matrix had started to degrade, changes in the peaks associated with the functional groups of PEEK would be expected. However, hardly any change can be detected in the spectrum of the nanocomposite upon irradiation. In particular, the carbonyl index,[33] calculated as the ratio of the area of the carbonyl peak to the area of a reference band (unchanging) at 1490 cm^{-1}, was 0.104 and 0.108 prior and after UV illumination, respectively, indicating the negligible formation of carbonyl groups under irradiation. Therefore, the FT-IR study corroborates the high UV resistance of these hybrid biomaterials, likely related to the excellent scattering and absorption properties of TiO_2 at UV wavelengths.[23]

Crystalline Structure. The influence of the nanoparticles on the crystalline structure of the matrix was explored by XRD, and the patterns of nano-TiO_2, neat PEEK, PEI, PEEK/PEI (70/30 wt/wt %) blend, and the nanocomposites with 1.0 and 8.0 wt % TiO_2 concentration are displayed in Figure 3. The
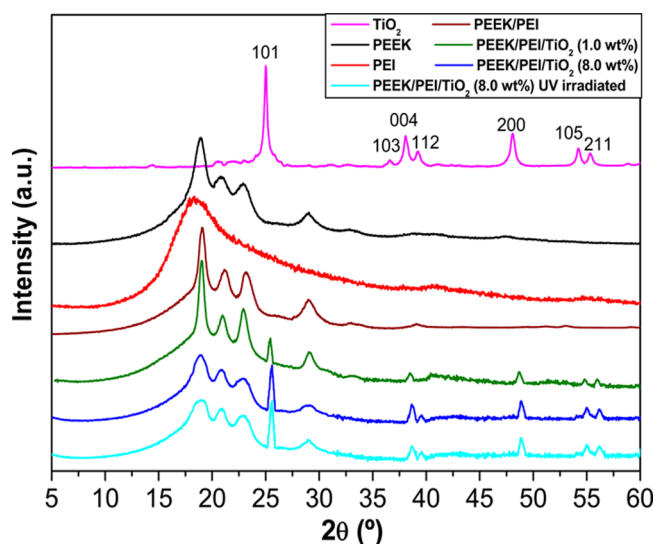
Figure 3. XRD patterns of bare TiO_2, PEEK, PEI, PEEK/PEI (70/30 wt/wt %) blend, and the nanocomposites with 1.0 and 8.0 wt % TiO_2. The XRD of PEEK/PEI/TiO_2 (8.0 wt %) after UV irradiation for 24 h is also included.

nanoparticles present typical peaks at 2θ values of 25.1°, 36.7°, 38.1°, 39.2°, 48.0°, 54.2°, and 55.3°, consistent with the standard JCPDS card no. 21−1272 (anatase TiO_2). Further, the strong diffraction peaks at 25.1° and 48.0° confirm its tetragonal anatase structure. The absence of spurious diffractions indicates the crystallographic purity, and the sharp crystalline reflections corroborate the crystallinity of the nanoparticles. Their mean crystallite size was calculated as 20.8 nm using the Scherrer equation.[36]

Regarding the biopolymers, the diffractogram of semicrystalline PEEK presents main reflections at 2θ values of 18.8°, 20.7°, 22.9°, and 28.9°, corresponding to the scattering of the (110), (111), (200), and (211) lattice planes of the orthorhombic unit cell.[37] In contrast, the diffractogram of PEI displays a single broad reflection in the range of $2\theta = 10−30°$ that reflects its amorphous character. The pattern of the PEEK/PEI blend is qualitatively similar to that of PEEK, albeit with narrower and more intense peaks, indicating an increase in the level of crystallinity of the polymer, which is interesting taking into

account that PEI is an amorphous polymer miscible with PEEK. This is a typical characteristic of miscible and compatible blends incorporating one noncrystallizing polymer.[20] Nevertheless, the crystalline structure of PEEK remains merely unaltered, since no shift in the position of the Bragg reflections is found.

The nanocomposites present the diffraction peak characteristics of both PEEK and TiO_2. The reflections arising from the matrix phase appear at the same 2θ values as those of the PEEK/PEI blend, though they show increased and decreased intensity in the nanocomposites with 1.0 and 8.0 wt % loading, respectively. In fact, a rise in crystallinity is observed for the sample with the lowest nanoparticle concentration together with a small diminution in the average crystallite size, while the opposite trend is found for that with the highest TiO_2 content. These results suggest a change from promotion to retardation in the crystallization rate of the polymer with increasing nanoparticle loading, which should be confirmed by DSC analysis. Thus, at low TiO_2 loading the nucleating effect of the nanoparticles likely leads to higher degree of crystallinity and smaller crystals, whereas at higher nanofiller concentration the increased TiO_2-matrix interactions could prevail over the nucleation effect, and the result is a drop in the overall level of crystallinity and in the size of the crystalline domains. An analogous phenomenon has been reported for PEEK composites reinforced with inorganic WS_2 nanoparticles, where the nucleation of the polymer crystals was only favored at low nanofiller contents.[15]

On another note, a gradual upshift in the position of the crystalline reflections arising from the nanoparticles is found with increasing TiO_2 content, hinting toward a modification in the dimensions of the anatase unit cell. Moreover, upon increasing nanofiller loading the peaks become steadily broader, indicative of a drop in the crystallite size, the diminution being ~20% for the nanocomposite with 8.0 wt % TiO_2. The steric impediment of the polymeric segments located nearby the nanoparticles might disturb their molecular packing, leading to smaller and more imperfect crystals. Nonetheless, these results should be taken with caution given the number of factors that can influence the width of the reflections; hence, the Scherrer equation only gives a lower limit of crystallite size.[36]

The effects of UV irradiation on the crystalline structure of the nanocomposites was also investigated, and the XRD of PEEK/PEI/TiO_2 (8.0 wt %) recorded after illumination with 365 nm UV light for 24 h is shown in Figure 3. No significant change is observed compared to the diffractogram of the nonirradiated nanocomposite, indicating that the degree of crystallinity and the crystallite size remain merely invariant. This supports the good UV radiation stability of these biocomposites, ascribed to the high UV-blocking capacity of TiO_2 nanoparticles.

Crystallization and Melting Behavior. DSC was employed to analyze the effect of TiO_2 on the crystallization and melting behavior of PEEK in the nanocomposites. The nonisothermal DSC thermograms are displayed in Figure 4, and the calorimetric parameters obtained from the thermograms are collected in Table 1. The crystallization temperature (T_c) of pure PEEK is ~304 °C. Interestingly, the addition of PEI leads to a small rise in T_c and also increases the level of crystallinity (X_c) (Figure 4a), consistent with the results from XRD. Regarding the ternary composites with low TiO_2 loadings (1.0 and 2.0 wt %), an increase in both T_c and X_c compared to those of the PEEK/PEI blend is observed, indicating that the nanoparticles accelerate the crystallization of PEEK due to
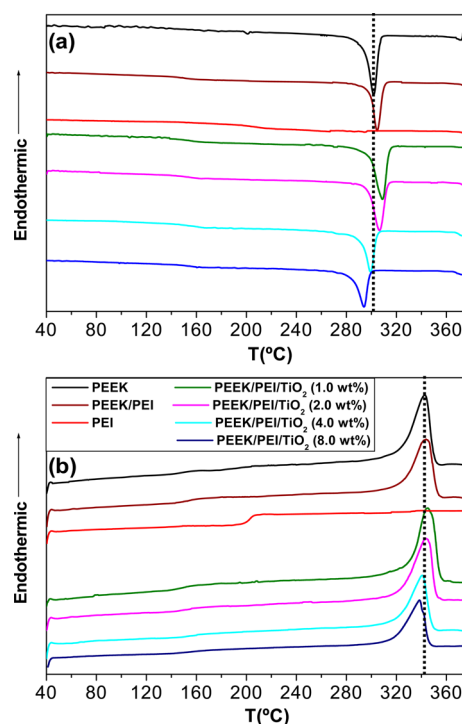
Figure 4. (a) Cooling and (b) heating DSC thermograms of PEEK, PEI, PEEK/PEI (70/30 wt/wt %) blend, and the nanocomposites with different TiO_2 contents.

heterogeneous nucleation effect. However, composites with higher nanofiller concentration display an opposite behavior, since both parameters significantly drop compared to the reference blend. One explanation for this phenomenon could be that the nanoparticles had a 2-fold effect: on the one hand, due to their large specific surface area and homogeneous dispersion within the matrix, they can effectively act as nucleating agents, thereby increasing the level of crystallinity and crystallization temperature. On the other hand, the OH groups of the nanoparticle surface can strongly interact both with PEEK and PEI, as explained earlier, and these interactions should impose important constraint on polymer chain diffusion and crystal growth, thus slowing the overall crystallization process. It appears that when a low amount of nanoparticles is added to the polymeric matrix, the nucleating effect predominates, while at higher contents, the restriction on polymer chain mobility predominates, and the overall result is a fall in both X_c and T_c.

Focusing on the heating scans obtained after dynamic crystallization (Figure 4b), qualitatively similar trends are detected. The melting temperature (T_m) is ~343 °C for neat PEEK and increases slightly in the PEEK/PEI blend. Nanocomposites with low nanoparticle loadings show higher T_m than the reference blend, while those with TiO_2 contents ≥4.0 wt % exhibit lower value. In this case, the strong restrictions of chain segmental mobility likely lead to smaller and less perfect crystals that melt at a lower temperature. On another note, a gradual rise in the glass transition temperature (T_g) is found on addition of increasing nanoparticle contents. However, it is difficult to accurately determine T_g values from DSC thermograms, and they have been measured from DMA.

Thermal Stability. Biomaterials for medical implant use can be subjected to elevated temperatures;[28] hence, a high heat resistance is required. The thermal stability of the developed

Table 1. Thermal Data^a Obtained from DSC and TGA Analyses of PEEK, PEI, PEEK/PEI (70/30 wt/wt%) blend, and the Nanocomposites with Different TiO$_2$ Content (values in parentheses)

material	T_c (°C)	T_m (°C)	X_c (%)	T_i (°C)	T_{10} (°C)	T_{max} (°C)	LOI (%)
PEEK	303.6	342.8	42.9	523.1	545.7	554.2	36.9
PEI				509.3	538.2	546.8	38.0
PEEK/PEI	305.0	343.3	45.4	524.6	547.9	557.4/631.2	38.4
PEEK/PEI/TiO$_2$ (1.0)	309.3	344.8	50.5	528.1	550.3	564.1/633.0	38.8
PEEK/PEI/TiO$_2$ (2.0)	307.5	344.0	47.2	535.3	557.6	570.2/627.2	39.3
PEEK/PEI/TiO$_2$ (4.0)	300.1	340.6	40.9	541.8	564.5	575.6/631.4	40.0
PEEK/PEI/TiO$_2$ (8.0)	296.2	338.1	38.1	548.0	568.1	578.8/625.7	41.1

$^a T_c$: crystallization temperature; T_m: melting temperature; X_c: degree of crystallinity; T_i: initial degradation temperature obtained at 2% weight loss; T_{10}: temperature for 10% weight loss; T_{max}: temperature of maximum rate of weight loss; LOI: limiting oxygen index.

nanocomposites was investigated by means of TGA under inert environment, and their decomposition curves together with those of neat PEEK, PEI, and the reference PEEK/PEI blend are shown in Figure 5a for comparison. Their characteristic
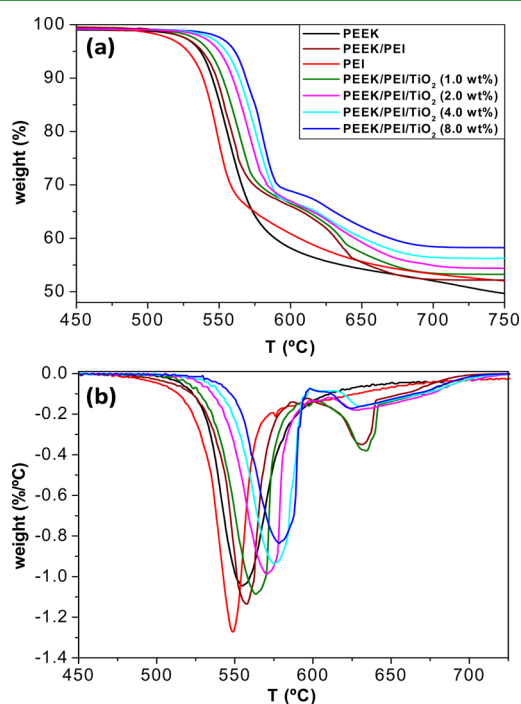

Figure 5. (a) TGA and (b) DTG curves under nitrogen atmosphere of the neat polymers, the PEEK/PEI blend, and the nanocomposites with different TiO$_2$ contents. For comparative purposes, only the temperature range between 450 and 750 °C is shown.

degradation temperatures are collected in Table 1. Both neat PEEK and PEI exhibit a single degradation stage under inert environment that initiates (T_i) at ~523 and 509 °C, respectively, and show the maximum rate of weight loss (T_{max}) at ~554 and 545 °C, as can be clearly observed from the differential thermogravimetric analysis (DTG) curves (Figure 5b). However, a two-step decomposition process is observed for the reference blend, in agreement with previous studies on the thermal degradation of PEEK/PEI binary mixtures.[38] Interestingly, this reference sample displays slightly higher degradation temperatures than PEEK, likely related to its higher level of crystallinity, since the increase in this property results in more thermally stable materials. The decomposition of the nanocomposites also takes place in two stages (Figure 5b), and their curves are similar to those of the matrix albeit shifted to

higher temperatures. Accordingly, both T_i and T_{max} increase with increasing TiO$_2$ concentration, the maximum increments being ~24 and 21 °C, respectively, for the nanocomposite with the highest nanoparticle loading. These noticeable improvements are related to the strong nanoparticle–matrix H-bonding interactions that hinder the mobility of the polymeric chains. Moreover, the nanoparticles can act as a barrier against the transport of volatile decomposed products.[11] Other factors contributing to the observed enhancement are the elevated thermal conductivity of TiO$_2$ that would favor heat dissipation within the sample and that this metal oxide is thermally stable up to 800 °C.[28]

TiO$_2$ nanoparticles not only boost the thermal stability of the matrix but also promote char residue formation. Char residues under inert atmosphere are related to the flame-retardant capability of the samples by the limiting oxygen index (LOI),[28] which can be estimated using Van-Krevelen and Hoftyzer equation,[39] and the calculated data are also listed in Table 1. A material is considered flammable when its LOI is ≤26%. Both PEEK and PEI are self-extinguishing polymers (LOI > 35%), and when burning, they give off very low amounts of smoke. The LOI further rises on increasing TiO$_2$ concentration, and a maximum 7% increase compared to the reference blend is reached at 8.0 wt % loading. This superior fire resistance is likely related to the elevated thermal conductivity of TiO$_2$, as mentioned above. The presence of the nanoparticles enables a faster heat dissipation within the nanocomposite, which delays the time to reach the ignition point.

Water Absorption. Biomaterials are frequently subjected to steam sterilization cycles; hence, very high moisture resistance is required. In this regard, water absorption kinetics of the fabricated nanocomposites was explored, and the results are displayed in Figure 6. A nonlinear growth of this property upon increasing time can be observed for all the samples, reaching a constant value (equilibrium) after one week. Pure PEEK displays a very low water absorption of ~0.13% at 24 h and ~0.42% at the equilibrium, while PEI exhibits higher values, about 0.18% and 0.52%, respectively. More interesting, the reference PEEK/PEI blend displays reduced absorption when compared to both polymers, likely associated with its higher degree of crystallinity, since the crystalline regions increase the tortuosity of the transport path. The incorporation of low TiO$_2$ loadings further decreases the water absorption rate, the reduction at the equilibrium being ~14 and 20% at 1.0 and 2.0 wt % loading, respectively, compared to the PEEK/PEI mixture. These data indicate that the nanocomposites have enhanced barrier performance against water, attributed to their higher level of crystallinity and the presence of homogeneously dispersed nanoparticles, facts that boost the tortuosity of
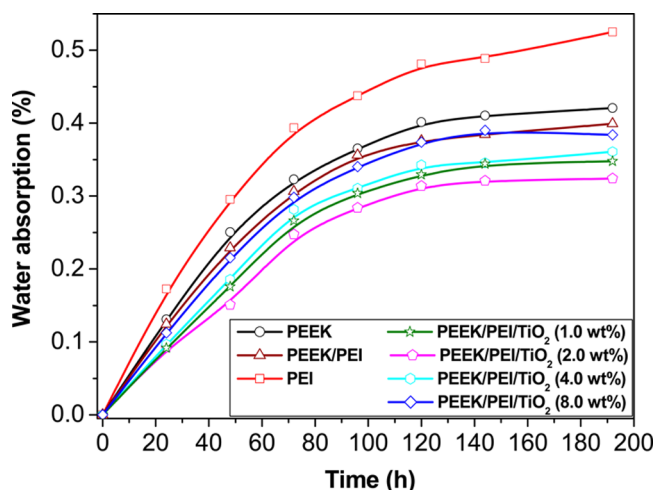
Figure 6. Water absorption kinetics of the pure polymers, the reference blend, and the TiO$_2$-reinforced nanocomposites.

Figure 7. (a) Storage modulus E' and (b) tan δ vs temperature for the neat polymers, the PEEK/PEI (70/30 wt/wt %) blend, and the nanocomposites with the indicated TiO$_2$ contents.

diffusion pathways within the matrix. Nonetheless, the incorporation of higher nanoparticle concentrations leads to smaller drops in the water absorption (i.e., ∼10% at 4.0 wt % TiO$_2$), and the composite with the highest nanofiller loading displays almost the same values as the reference blend, suggesting that other factors influence the water absorption. Indeed, TiO$_2$ nanoparticles are much more hydrophilic than the neat polymers; hence, the hydrophilicity of the nanocomposites would rise upon increasing nanoparticle loading. Moreover, the degree of nanoparticle dispersion also affects the barrier properties, given that the presence of small clusters can lead to preferred paths for water diffusion.[40] Overall, the behavior observed probably arises from a balance between nanocomposite water affinity, level of crystallinity, nanoparticle dispersion, and tortuosity effects.

Dynamic Mechanical Performance. The dynamic mechanical properties of the nanocomposites were investigated by DMA, and the temperature dependence of their storage modulus (E') and loss factor (tan δ) at the frequency of 1 Hz is shown in Figure 7. For comparison, data of the neat polymers and the reference blend are also plotted. The T_g and E' values at different temperatures are listed in Table 2.

At 25 °C, E' of neat PEEK is ∼3.7 GPa (Figure 7a) and decreases gradually upon increasing temperature, showing a sharp drop in the vicinity of the T_g. The rise in temperature results in increased chain mobility and hence in an E' fall, especially at temperatures in the vicinity and higher than the T_g where whole segmental motion takes place. An analogous behavior is found for neat PEI, a rigid amorphous thermoplastic with a storage modulus of ∼3.4 GPa at 25 °C that softens at temperatures above 200 °C, showing a pronounced modulus reduction. E' of the PEEK/PEI (70/30 wt/wt %) mixture is slightly higher than that of pure PEEK in most of the temperature range, consistent with the higher degree of crystallinity of the blend, given that the crystalline regions increase E' of semicrystalline polymers.[5] Clearly, E' of the nanocomposites rises with the incorporation of TiO$_2$ at temperatures both below and above the T_g (Figure 7a), demonstrating the nanoparticle-induced matrix stiffening. In particular, at room temperature, the incorporation of 1.0, 2.0, 4.0, and 8.0 wt % TiO$_2$ contents raises E' of the blend by 18, 29, 37, and 41%, respectively. These results reveal a nonlinear growth of the modulus with the nanoparticle concentration, the
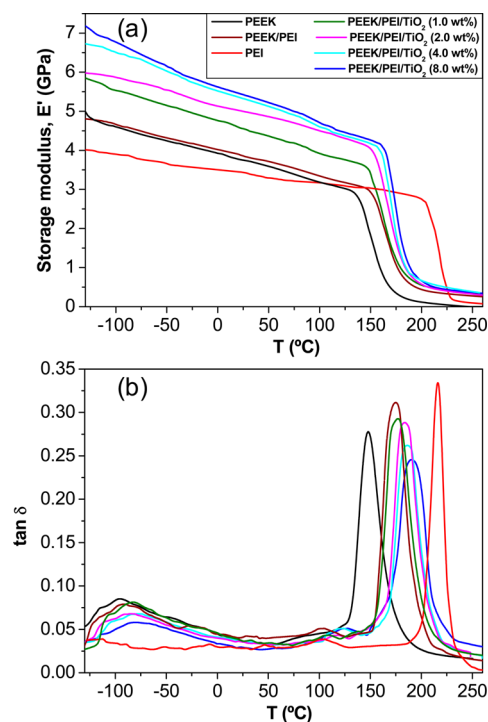
increment being more prominent at low loadings. The strong E' improvement attained with the addition of 1.0 and 2.0 wt % TiO$_2$ is attributed to the rise in crystallinity due to heterogeneous nucleation together with the reinforcement effect. However, the enhancements obtained at higher loadings should merely be related to conventional reinforcement effects, since the crystallinity of such nanocomposites is lower than that of the matrix (see Table 1). The stiffening effect of the nanoparticles is even more prominent above the T_g of the blend (i.e., ∼33 and 57% rise at 200 °C for the nanocomposites with 1.0 and 8.0 wt %, respectively, see Table 2). Similar trend was found for PEEK nanocomposites reinforced with other inorganic nanoparticles such as ZnO[11] or WS$_2$.[15]

The tan δ (ratio of the loss to storage modulus) is a measure of the damping within the system and is very sensitive to the material morphology. The development of the tan δ as a function of temperature (Figure 7b) shows two transition peaks for neat PEEK: that at the lowest temperature (centered around −95 °C), named β-transition, is ascribed to local motions of the ketone groups, while the relaxation at the highest temperature (∼148 °C), named α-transition, corresponds to the T_g. Neat PEI also displays two transition temperatures, the β-relaxation at ∼100 °C related to the movement of the imide groups and the α-transition at ∼217 °C.[41] The PEEK/PEI blend also exhibits relaxation peaks at ca. −92 and 100 °C, and a single α-relaxation at 174 °C, which corroborates the homogeneous miscibility of the two polymers in the amorphous phase. Interestingly, the T_g of the blend is ∼26 °C higher than that of neat PEEK, upshift greater than the predicted by the Fox equation[42] for homogeneous mixtures (∼20 °C). The discrepancy should arise from the change in the composition of the amorphous phase due to the increase in the degree of crystallinity of PEEK. Thus, T_g rises with increasing crystallinity, since the segmental motion in the amorphous

Table 2. DMA Data^a for the Different Samples

material	T_g (°C)	$E'_{-100 °C}$ (GPa)	$E'_{25 °C}$ (GPa)	$E'_{200 °C}$ (MPa)	tan δ_{max} (a.u.)	fwhm (°C)	tan δ_{area} (a.u.)
PEEK	148.1	4.59	3.73	0.130	0.28	24.2	5421
PEI	216.6	3.88	3.44	2.721	0.33	16.0	4192
PEEK/PEI	174.0	4.65	3.86	0.419	0.31	27.3	6718
PEEK/PEI/TiO$_2$ (1.0)	176.2	5.50	4.56	0.559	0.29	27.5	6980
PEEK/PEI/TiO$_2$ (2.0)	183.8	5.84	4.98	0.582	0.28	28.7	6840
PEEK/PEI/TiO$_2$ (4.0)	185.5	6.47	5.31	0.637	0.26	28.0	6256
PEEK/PEI/TiO$_2$ (8.0)	190.3	6.75	5.45	0.658	0.24	32.3	8590

$^a T_g$: glass transition temperature; E': storage modulus; tan δ_{max}: height of tan δ peak; fwhm: full-width at half-maximum of tan δ peak; tan δ_{area}: area under tan δ peak.
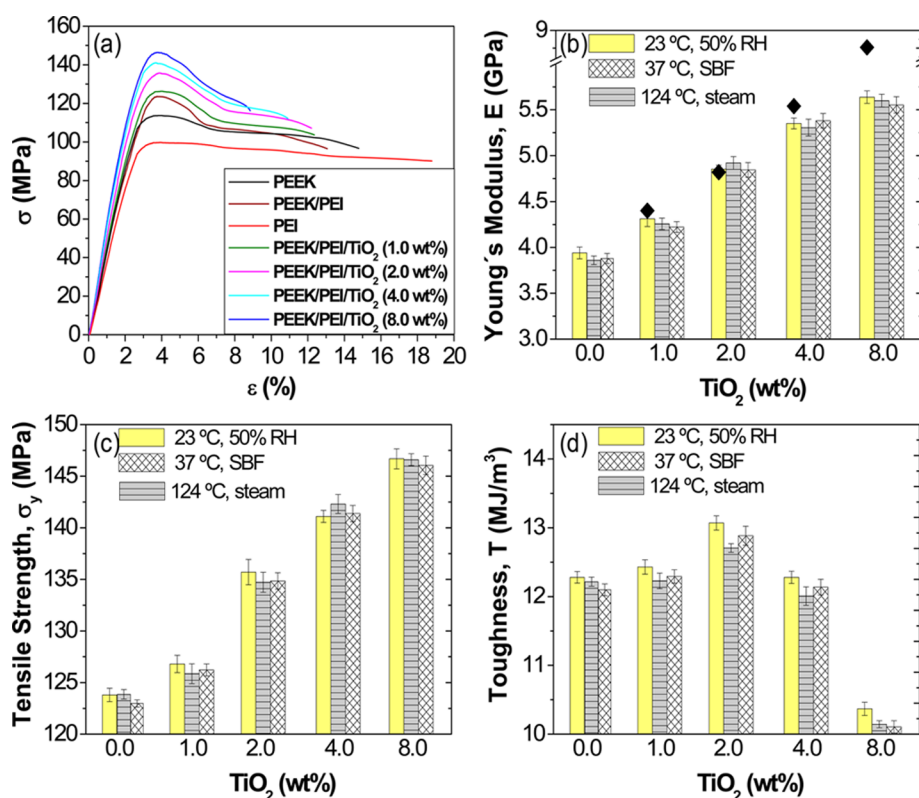
Figure 8. (a) Stress—strain curves of the indicated samples at room temperature. Young's modulus (b), tensile strength (c), and toughness (d) of PEEK/PEI/TiO$_2$ nanocomposites with different nanoparticle loadings under different environmental conditions (see explanation in the text). The solid symbols in (b) correspond to the theoretical values calculated using the Krenchel's model.

phase is decreased near the crystal lamellae. Further, a broadening of the glass transition feature is detected when compared with the spectra of the pure polymers, consistent with the observations by Goodwin and Simon,[41] who ascribed such phenomenon to concentration fluctuations and larger range of coupled interactions in the mixture.

The addition of TiO$_2$ to the PEEK/PEI mixture causes a significant increase in the relaxation temperatures, particularly in the T_g, which rises by ~16 °C for the nanocomposite with the highest nanoparticle concentration (Table 2). This noticeable increment is ascribed to the formation of a nanoparticle network that hinders the mobility of the polymer segments and reduces the free volume. Further, the effective chain motion restriction should be related to the strong H-bonding interactions between the polymers and TiO$_2$ together with the homogeneous nanoparticle distribution that leads to a large matrix-nanofiller interfacial contact area. The T_g increments observed in this work are higher than those found upon incorporation of other inorganic nanoparticles such as ZnO[11] or

WS$_2$[15] to PEEK, likely due to the presence of PEI that acts as a coupling agent, strengthening the interactions between the composite components. Moreover, a widening of the tan δ peak is detected, especially for the nanocomposite with the highest nanoparticle loading (Table 2), which displays a full-width at half-maximum (fwhm) value ~5 °C higher than that of the reference blend. This widening effect is most likely caused by the difference between the physical states of polymeric segments in the vicinity of the nanoparticles that are hindered in their mobility compared to the less-constrained segments of the bulk matrix. Similar behavior has been reported for other nanofiller-reinforced PEEK composites[9] and is typical for polymer systems filled with finely dispersed materials. In addition, a gradual drop in the height of the tan δ peak is found upon increasing nanoparticle concentration, by up to 22% at 8.0 wt % loading (Table 2), related to the reduced fraction of polymer matrix. Besides, the magnitude of the tan δ indicates the level of viscosity of a system: the lower the tan δ, the higher the elasticity of the material. Hence, the reduced tan δ peak

height in the nanocomposites suggests that when the tension is eliminated the energy stored during the deformation process recuperates at a higher speed compared to the unfilled polymer mixture.

On another note, noticeable changes in the area under the tan δ peak are found with the incorporation of the nanoparticles (Table 2), which can be associated with the modification of the impact strength of the material.[5] All the nanocomposites display similar or even bigger area than the polymer blend, reaching a maximum increase of 28% at 8.0 wt % TiO$_2$. These results point toward an increase in energy dissipation with increasing nanoparticle concentration and suggest that these inorganic nanofillers can simultaneously improve the stiffness and impact resistance of the matrix.

Static Mechanical Properties. Composites to be used for load-bearing implant applications demand high modulus, strength, and toughness. In this regard, the static mechanical properties of TiO$_2$-reinforced PEEK/PEI ternary nanocomposites were investigated by means of tensile tests, and typical stress−strain curves are shown in Figure 8a. Their room-temperature Young's modulus (E), tensile strength (σ_y), and toughness (T) values derived from the curves are compared in Figure 8b−d. Neat PEEK and PEI show a Young's modulus of ~4.0 and 3.5 GPa, respectively. The addition of 30 wt % of PEI to semicrystalline PEEK leads to changes in the mechanical deformation behavior. While the elastic modulus remains merely unchanged, the blend displays higher tensile strength and a more pronounced "yield-drop", together with decreased strain at break. The rise in tensile strength correlates with the higher degree of crystallinity of the blend, while the increased necking behavior and the reduced elongation at break should arise from the PEI-enriched amorphous regions of the blend. Regarding the nanocomposites, a gradual increase in both E and σ_y is found on increasing TiO$_2$ content, showing maximum improvements of 41% (Figure 8b) and 19% (Figure 8c), respectively, at the highest loading tested. These noticeable enhancements can be ascribed to the reinforcement effect of the stiff and homogeneously dispersed TiO$_2$ nanofillers combined with the presence of PEI that acts as a coupling agent and strengthens the PEEK-nanoparticle interfacial adhesion via polar and H-bonding interactions. Note that the stiffness and strength enhancements observed in this study are higher than those found for PEEK nanocomposites reinforced with other inorganic nanofillers like SiO$_2$, Al$_2$O$_3$, and WS$_2$.[9,10,15] To the best of our knowledge, only nanocomposites incorporating low amounts (~1.0 wt %) of single-walled carbon nanotubes grafted to a PEEK derivative displayed superior rigidity, which can be understood taking into account the outstanding modulus of this carbon nanofiller (~1 TPa).

Taking the reported value for the Young's modulus of TiO$_2$ nanoparticles (230 GPa),[23] the theoretical E data for the nanocomposites were calculated following the Krenchel's model[5] (see solid symbols in Figure 8b). Experimental E data are in very good agreement with the predictions (differences <4%) up to TiO$_2$ loadings of 4.0 wt %. However, at a higher concentration, the experimental value falls well below the theoretical one, which could be related to the noticeable drop in the level of crystallinity of the matrix. In fact, the model assumes that the modulus of each composite phase is unaffected by the presence of the other components; conversely, results have shown that high amounts of nanoparticles hinder the matrix crystallization. Therefore, in the nanocomposite with the highest loading, the properties of

PEEK might differ from those of the neat polymer, and this might account for the discrepancy between the theoretical and the experimental data.

On the other hand, the elongation at break shows a gradual decrease with increasing nanoparticle content, the drop being more prominent at higher loadings (i.e., ~31% for the nanocomposite with 8.0 wt % TiO$_2$). This behavior is typical of nanofiller-reinforced composites, since the fillers obstruct plastic deformation of the matrix, thereby leading to lower ductility. Nonetheless, for similar nanoparticle concentration, the reduction in tensile strain found for Al$_2$O$_3$ or SiO$_2$-reinforced PEEK nanocomposites was significantly stronger (close to 70%), ascribed to severe nanoparticle clustering.[10] The presence of PEI helps to prevent nanoparticle aggregation, making the reduction in ductility less drastic. More interesting are the toughness data derived from the tensile curves (Figure 8d). The incorporation of low TiO$_2$ content provokes a small toughness improvement, leading to a maximum increment of ~8% at 2.0 wt % loading. The homogeneously and individually dispersed nanoparticles can efficiently stop crack propagation, leading to improved impact strength. Conversely, the addition of more than 4 wt % TiO$_2$ makes the nanocomposites more brittle, likely due to the presence of small particle clusters that may act as stress concentration sites and initiate the cracks, causing an earlier failure.

Any biomaterial intended to be used as a medical implant should withstand the body environment, and hence should retain the properties after long-term exposure to SBF at 37 °C. Moreover, it should resist numerous cycles in an autoclave, an approach frequently employed for sterilization of medical implants. In this regard, the mechanical properties of the nanocomposites were investigated under such conditions, and the results are also plotted in Figure 8. Interestingly, E and σ_y values of all the nanocomposites remain unaltered after sterilization or exposure to SBF (differences ≤2%), whereas the toughness exhibits a small reduction (<4%), although the variations are within the standard deviations of the measurements. Experimental results demonstrate that both the exposure to SBF and the autoclaving (steam sterilization) have an insignificant effect on the tensile properties of these nanomaterials, consistent with the exceptional environmental resistance of both PEEK and PEI.[43] Consequently, the developed biomaterials seem suitable for long-term implant applications, which is of great interest, since the use of this type of implant significantly reduces the number of operative procedures and improves the quality of patient life.[44]

Tribological Properties. The tribological performance of biomaterials is of outmost importance; they should meet various requirements such as low coefficient of friction and resistance to wear and abrasion. The presence of wear debris produced when a bone rubs against the implant may result in inflammation and osteolysis,[45] leading to loosening of prostheses and necessitating revision surgery. To assess the tribological behavior of the ternary nanocomposites, their coefficient of friction (μ) and specific wear rate (W_{sp}) were measured under both dry conditions at 23 °C and SBF environment at 37 °C, and the results are presented in Figure 9a,b, respectively.

Under dry conditions, μ of PEEK is ~0.35, and that of PEI ~0.42, while that of the PEEK/PEI (70/30 wt/wt %) blend is smaller (~0.33), related to the increase in crystallinity of the blend. This is consistent with previous studies on the tribological behavior of semicrystalline thermoplastics that
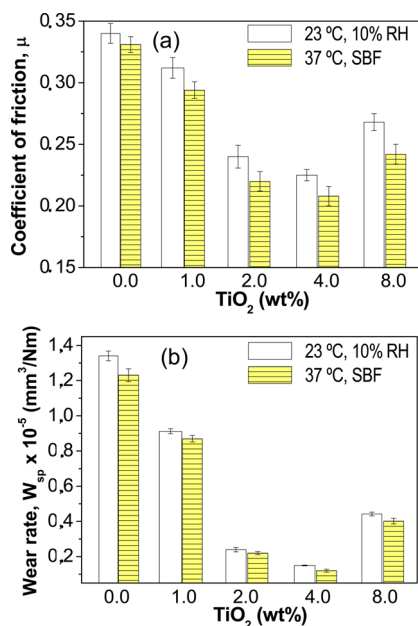
Figure 9. (a) Coefficient of friction and (b) specific wear rate under dry and SBF conditions of PEEK/PEI/TiO$_2$ nanocomposites.

found reduced μ for samples with higher level of crystallinity.[46] The incorporation of TiO$_2$ gradually reduces μ of the blend, by as much as 34% at 4.0 wt % content. The nanoparticles are believed to have two main functions: promote crystallization and act as crack deflectors. At low nanoparticle loadings, both the amount of nucleation sites and the surface area available for crack deflection increase. However, at higher loadings, the presence of small clusters limits the effectiveness of the nanoparticles, resulting in smaller μ diminution. Very similar trend is found under SBF condition, where μ falls from ~0.32 for the PEEK/PEI reference blend to ~0.21 for the nanocomposite with 4.0 wt % TiO$_2$ concentration, in agreement with the fact that the reinforcing effect of the nanoparticles is almost the same under dry and lubricated environments (Figure 8). For all the samples, μ is lower in SBF conditions, related to the lubricating effect of the aqueous medium.[28] This behavior is consistent with the results reported by Unal and Mimaroglu,[47] who compared the tribological performance of PEEK and PEI-reinforced composites under dry and lubricated conditions. Further, the interaction of the polymers with water and the surface wettability can influence the tribological behavior of the samples in an aqueous environment.

The PEEK/PEI blend shows a W_{sp} value in dry conditions of ~1.3 × 10^{-5} mm^3/Nm, also lower than that of the pure polymers (~2.5 × 10^{-5} and 1.0 × 10^{-4} mm^3/Nm for PEEK and PEI, respectively). The addition of TiO$_2$ further decreases this property, leading to ~10-fold decrease at 4.0 wt % loading, while at higher concentrations the improvement in wear resistance was smaller. An analogous trend has been reported for PEEK nanocomposites reinforced with other inorganic nanoparticles such as Si$_3$N$_4$, SiC, SiO$_2$, or ZrO$_2$,[48] where the minimum W_{sp} value was attained at a critical nanofiller content of ~2 vol %, ascribed to the formation of particle aggregates at higher concentrations that hinder the formation of a uniform and continuous transfer film on the countersurface.

On the other hand, it is found that W_{sp} in SBF environment is systematically lower than that under dry conditions, in

agreement with the study by Zhong et al.[49] who compared the wear performance of PEEK composites reinforced with SCFs and ZrO$_2$ nanoparticles in water and air and found that the surface damage was caused by scuffing under water lubrication, while, under dry sliding, microcracking was the predominant mechanism. Aqueous lubrication has advantages and disadvantages, and the overall positive or negative effect is determined by the nature of the polymeric matrix and the dominating mechanism involved in the sliding process. On the one hand, water absorption and plasticization of the polymer surface can take place in an aqueous medium, leading to changes in the surface structure by swelling, causing a diminution in the attractive forces between polymer segments and consequently to a fall in modulus and hardness that is reflected in decreased wear resistance. Nonetheless, experimental results have shown that PEEK and the nanocomposites have very low water absorption (Figure 6) and that their mechanical performance is nearly independent of the surrounding medium; therefore, the plasticization effect must be insignificant. Besides, in SBF condition the hydraulic action can perturb the development of the transfer layer, resulting in increased wear rate. On the other hand, aqueous solutions at polymer−metal contacts can act as cooling agents, reducing the shear strength due to water lubricant characteristics. The presence of water at the interface between the specimen and steel disc washes away the wear debris, which improves heat transfer and favors the formation of a hydrodynamic, full film lubricant layer between the polymeric chains and the countersurface, thereby leading to improved wear resistance. Therefore, it seems that the latter mechanism prevails in the nanocomposites studied in this work, and the overall result is a wear rate reduction in SBF medium.

Dielectric Properties. As known, the physiological processes in the tissues are joined to the flow of electric current through structural components such as intra- and extracellular fluids and charge buildup at the interface, which are feasibly owed to their dielectric properties. Thus, knowledge of the dielectric properties (a measure of the polarizability of a material when subjected to an electric field) is crucial for the development of biomaterials, particularly in the case of functional scaffolds for load-bearing applications.[50] TiO$_2$ possesses a high dielectric constant (~40 in the case of nanoparticles), which gives it the ability to bind to bone and living tissues, known as osseointegration.[51]
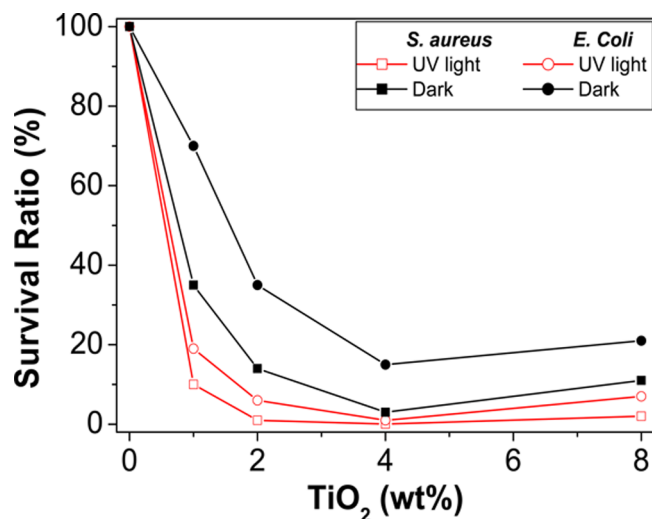
Figure 10 shows the evolution of the dielectric constant (ε'), which represents the material capability to store energy, and dielectric loss (ε''), which indicates the ability to dissipate the electric field energy versus frequency for neat PEEK, PEI, the reference blend, and the corresponding nanocomposites. The ε' value drops with increasing frequency, although it changes only slightly at frequencies >10^4 Hz. The high value of ε' at low frequencies is ascribed to space charge polarization.[29] However, as frequency rises the electron exchange is not able to follow the electric field, and the polarization becomes independent of frequency. The ε' value of PEEK is relatively low (~3 at 10 Hz) and remains almost constant at high frequencies. Similar behavior is found for PEEK/PEI blend, showing a slightly higher value. The addition of polar TiO$_2$ to PEEK/PEI causes a noticeable increase in ε' (Figure 10a), particularly at low frequencies (i.e., below 1 × 10^3 Hz). Thus, at 10 Hz, almost 2-fold increase is attained at the highest nanoparticle loading, attributed to the high ε' of TiO$_2$. Analogous phenomenon has been reported for epoxy/TiO$_2$ nanocomposites,[52] related to the high permittivity of TiO$_2$, which improves the polarization via
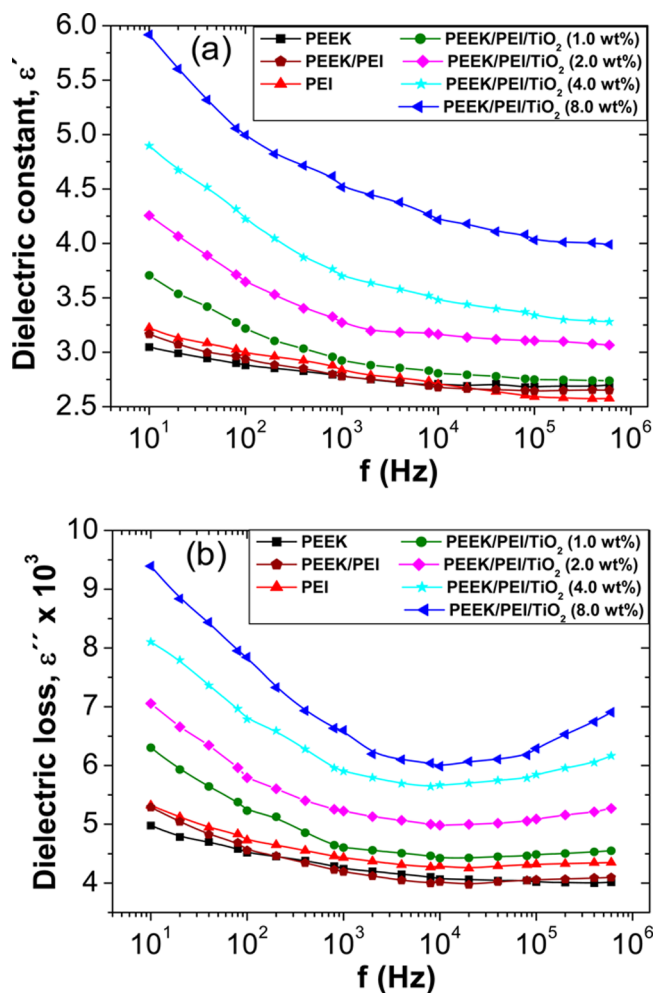
Figure 10. (a) Dielectric constant and (b) dielectric loss as a function of frequency for the indicated samples.

Figure 11. Antibacterial activity of the nanocomposites against *E. coli* and *S. aureus*. Solid and open symbols correspond to experiments performed without and with UV light, respectively.

dipole–dipole interactions among neighboring nanoparticles. Further, the nanocomposites show a marked increase in ε' with decreasing frequency. This is clearly related to the presence of the nanoparticles and suggests a Maxwell–Wagner interfacial polarization.[52] Similarly, ε'' rises gradually on increasing TiO_2 loading (Figure 10b), also related to the increase in the space charge density. Nonetheless, ε'' decreases with increasing frequency up to 10^4 Hz and then rises, this effect being more pronounced with increasing nanoparticle content. Overall, upon raising nanoparticle concentration the polarization is increased, which means that the nanocomposites are better dielectric materials for the development of tissue scaffolds than the neat polymers.

Antibacterial Activity. In this study, the antibacterial activity of the nanocomposites was explored against two bacteria that are pathogens of humans: *E. coli* (Gram-negative) and *S. aureus* (Gram-positive); the latter is among the most frequent reasons for postoperative infection. Experiments were carried out in the absence and in the presence of UV irradiation, and the results are plotted in Figure 11. As can be observed, PEEK/PEI sample, which was used as a control matrix, exhibited no antibacterial activity under any of the conditions. In all cases, the survival ratio decreases with increasing nanoparticle concentration, showing a minimum at 4.0 wt % TiO_2, and then rises slightly. This behavior could be explained considering that at low nanoparticle content, the

interaction of TiO_2 with the bacteria cell wall should be weak, while at high loadings the presence of small particle clusters reduces the effective surface-to-volume ratio of the nanofillers; hence, the TiO_2-bacteria interaction is decreased. Under UV illumination, *E. coli* activity is hindered when TiO_2 concentration is 4.0 wt %, while *S. aureus* growth is restrained by all the nanocomposites excluding that with 1.0 wt % loading. This is in agreement with previous studies on TiO_2-containing biofilms[53] that found a stronger antibacterial action against Gram-positive bacteria. When TiO_2 materials are irradiated with UV light, reactive oxygen species (ROS, i.e., O_2^-, HO_2, and HO radicals) are produced that cause the lysis of bacteria, and this is believed to be the main reason for TiO_2 toxicity.[54] The more effective inactivation of *S. aureus* should be attributed to structural and chemical compositional differences between the cell surfaces of Gram-positive and Gram-negative bacteria.[55] Thus, the former only possesses a peptidoglycan sheath in the exterior of the cytoplasmic membrane, while Gram-negative cell wall is denser, more complex, and contains an outer membrane that confers resistance to a large number of substances, reducing the damage from oxidation radicals.

In the absence of UV light, the nanocomposites are only slightly toxic to *E. coli* (~15% survival ratio at 4.0 wt % loading), even though they show noticeable antibacterial activity against *S. aureus* (~3% survival ratio at such optimal TiO_2 concentration), consistent with previous works that investigated the antibacterial activity of nano-TiO_2 without irradiation,[56,57] although the main reason for cytotoxicity without irradiation is still unclear. In this regard, various mechanisms have been proposed:[28,56] the nanoparticle adsorption onto the bacteria cell wall, redox reactions at the bacteria–nanoparticle interface causing the reduction of Ti(IV) to Ti(III), and the internalization of the nanoparticles in the cytoplasm and consequent cell death/damage. Moreover, proof for ROS formation at the bacteria surface without UV irradiation has also been provided.[57] Overall, qualitatively similar trends are found under both experimental conditions, suggesting that the optimal TiO_2 concentration for efficient inhibition of bacterial growth is 4.0 wt %.

4. CONCLUSIONS

A miscible PEEK/PEI biopolymer blend was used as matrix material for the development of nano-TiO$_2$ reinforced hybrid bionanocomposites. These were successfully prepared via ultrasonication followed by conventional melt-blending without using nanoparticle surface treatments or polymer functionalization. Their morphology, crystallization behavior, crystalline structure, water absorption, thermal, mechanical, tribological, dielectric, and antibacterial properties have been thoroughly analyzed. Uniform titania dispersion within the biopolymer blend was attained, as revealed by SEM observations, ascribed to the presence of PEI that acts as a coupling agent, interacting both with PEEK by $\pi-\pi$ stacking and polar interactions as well as with the nanoparticles via H-bonds. The incorporation of low TiO$_2$ loadings increased the crystallization temperature and the level of crystallinity of the PEEK/PEI blend, whereas at higher concentrations the restrictions on polymer chain mobility predominate, resulting in lower crystallinity and smaller crystallite size. A gradual increase in thermal stability and flame-retardant capability was observed upon increasing nanoparticle concentration. The nanocomposites exhibited lower water absorption than the reference blend, since the homogeneously dispersed nanoparticles increase the tortuosity of diffusion pathways within the matrix. They also displayed superior storage and Young's modulus, tensile strength, toughness, and glass transition temperature while reducing coefficient of friction and wear rate, and the optimal combination of properties was obtained at 4.0 wt % TiO$_2$. The enhanced mechanical properties of the nanocomposites and the strong TiO$_2$-matrix interfacial adhesion attained in the presence of PEI are believed to be the main reasons for the improvements in tribological properties observed under both dry and SBF conditions. Further, the tensile properties remained unaffected after exposure to a number of cycles of steam sterilization in an autoclave or to SBF at 37 °C. Both the dielectric constant and the dielectric loss raised gradually on increasing TiO$_2$ loading, ascribed to the rise in the space-charge density. The nanocomposites showed significant antibacterial properties against human pathogenic bacteria with and without UV illumination, and the effect on *S. aureus* was systematically stronger than that on *E. coli.* These novel hybrid biomaterials are potentially useful for long-term load-bearing implant applications like bone substitutes, spinal implants, hip replacements, or lumbar intervertebral body fusion cages due to their enhanced mechanical, tribological, thermal, and dielectric properties combined with their antibacterial characteristics.

■ AUTHOR INFORMATION

Corresponding Author
*E-mail: am.diez@uah.es.

Notes
The authors declare no competing financial interest.

■ ACKNOWLEDGMENTS

■ REFERENCES

(1) Liu, X. Y.; Chu, P. K.; Ding, C. X. Surface Modification of Titanium, Titanium Alloys, and Related Materials for Biomedical Applications. *Mater. Sci. Eng. R* **2004**, *47*, 49−121.

(2) Sagomonyants, K. B.; Jarman-Smith, M. L.; Devine, J. N.; Aronow, M. S.; Gronowicz, G. A. The in Vitro Response of Human Osteoblasts to Polyetheretherketone (PEEK) Substrates Compared to Commercially Pure Titanium. *Biomaterials* **2008**, *29*, 1563−1572.

(3) Teoh, S. H.; Tang, Z. G.; Hastings, G. W. In *Thermoplastic Polymers in Biomedical Applications: Structures, Properties and Processing*, Handbook of Biomaterial Properties; Springer: New York, 1998; pp 270−301.

(4) Kurtz, S. M.; Devine, J. N. PEEK Biomaterials in Trauma, Orthopedic, and Spinal Implants. *Biomaterials* **2007**, *28*, 4845−4869.

(5) Diez-Pascual, A. M.; Naffakh, M.; Gonzalez-Dominguez, J. M.; Ansón, A.; Martinez-Rubi, Y.; Martinez, M. T.; Simard, B.; Gómez, M. A. High Performance PEEK/Carbon Nanotube Composites Compatibilized with Polysulfones-II. Mechanical and Electrical Properties. *Carbon* **2010**, *48*, 3500−3511.

(6) Jones, D. P.; Leach, D. C.; Moore, D. R. Mechanical Properties of Poly(ether-ether-ketone) for Engineering Applications. *Polymer* **1985**, *26*, 1385−1393.

(7) Bakar, A. M. S.; Cheng, M. H. W.; Tang, S. M.; Yu, S. C.; Liao, K.; Tan, C. T.; Khor, K. A.; Cheang, P. Tensile Properties, Tension-Tension Fatigue and Biological Response of Polyetheretherketone-Hydroxyapatite Composites for Load-Bearing Orthopedic Implants. *Biomaterials* **2003**, *24*, 2245−2250.

(8) Yu, S.; Hariram, K. P.; Kumar, R.; Cheang, P.; Aik, K. K. In Vitro Apatite Formation and its Growth Kinetics on Hydroxyapatite/Polyetheretherketone Biocomposites. *Biomaterials* **2005**, *26*, 2343−2352.

(9) Díez-Pascual, A. M.; Naffakh, M.; Marco, C.; Ellis, G.; Gómez-Fatou, M. A. High-Performance Nanocomposites based on Polyetherketones. *Prog. Mater. Sci.* **2012**, *57*, 1106−1190.

(10) Kuo, M. C.; Tsai, C. M.; Huang, J. C.; Chen, M. PEEK Composites Reinforced by Nano-sized SiO$_2$ and Al$_2$O$_3$ Particulates. *Mater. Chem. Phys.* **2005**, *90*, 185−195.

(11) Diez-Pascual, A. M.; Xu, C. P.; Luque, R. Development and Characterization of Novel Poly(ether ether ketone)/ZnO Bionanocomposites. *J. Mater. Chem. B* **2014**, *2*, 3065−3078.

(12) Diez-Pascual, A. M.; Diez-Vicente, A. L. Development of Nanocomposites Reinforced with Carboxylated Poly(ether ether ketone)-grafted to Zinc Oxide with Superior Antibacterial Properties. *ACS Appl. Mater. Interfaces* **2014**, *6*, 3729−3741.

(13) Wang, Q.-H.; Xu, J.; Shen, W.; Xue, Q. The Effect of Nanometer SiC Filler on the Tribological Behavior of PEEK. *Wear* **1997**, *209*, 316−321.

(14) Balaji, V.; Tiwari, A. N.; Goyal, R. K. Fabrication and Properties of High Performance PEEK/Si$_3$N$_4$ Nanocomposites. *J. Appl. Polym. Sci.* **2011**, *119*, 311−318.

(15) Naffakh, M.; Diez-Pascual, A. M.; Marco, C.; Gómez, M. A.; Jiménez, I. Novel Melt-Processable Poly(ether ether ketone)(PEEK)/Inorganic Fullerene-like WS$_2$ Nanoparticles for Critical Applications. *J. Phys. Chem. B* **2010**, *114*, 11444−11453.

(16) Naffakh, M.; Diez-Pascual, A. M. Nanocomposite Biomaterials based on Poly(ether-ether-ketone) (PEEK) and WS$_2$ Inorganic Nanotubes. *J. Mater. Chem. B* **2014**, *2*, 4509−4520.

(17) Díez-Pascual, A. M.; Naffakh, M.; Gómez, M. A.; Marco, C.; Ellis, G.; Martinez, M. T.; Anson, A.; Gónzalez-Domínguez, J. M.; Martinez-Rubi, Y.; Simard, B.; Ashrafi, B. The Influence of a Compatibilizer on the Thermal and Dynamic Mechanical Properties of PEEK/Carbon Nanotube Composites. *Nanotechnology* **2009**, *20*, 315707−315715.

(18) Yano, K.; Usuki, A.; Okada, A.; Kurauchi, T.; Kamigaito, O. Synthesis and Properties of Polyimide-Clay Hybrid. *J. Polym. Sci., Part A: Polym. Chem.* **1993**, *31*, 2493−2498.

(19) Bijwe, J.; Tewari, U. S.; Vasudevan, P. Friction and Wear of Bulk Polyetherimide. *J. Mater. Sci.* **1990**, *25*, 548−556.

(20) Harris, J. E.; Robeson, L. M. Miscible Blends of Poly(aryl ether ketone)s and Polyetherimides. *J. Appl. Polym. Sci.* **1988**, *35*, 1877−1891.

(21) Torre, L.; Kenny, J. M. Blends of Semicrystalline and Amorphous Polymeric Matrices for High Performance Composites. *Polym. Compos.* **1992**, *13*, 380−385.

(22) Frigione, M.; Naddeo, C.; Acierno, D. Crystallization Behavior and Mechanical Properties of Poly(aryl ether ether ketone)/Poly(ether imide) Blends. *Polym. Eng. Sci.* **1996**, *36*, 2119−2128.

(23) Chen, X.; Mao, S. S. Titanium Dioxide Nanomaterials: Synthesis, Properties, Modifications, and Applications. *Chem. Rev.* **2007**, *107*, 2891−2959.

(24) Visai, L.; De Nardo, L.; Punta, C.; Melone, L.; Cigada, A.; Imbriani, M.; Arciola, C. R. Titanium Oxide Antibacterial Surfaces in Biomedical Devices. *Int. J. Artif. Organs* **2011**, *34*, 929−946.

(25) Gutwein, L. G.; Webster, T. J. Osteoblast and Chondrocyte Proliferation in the Presence of Alumina and Titania Nanoparticles. *J. Nanopart. Res.* **2002**, *4*, 231−238.

(26) Lu, X.; Lv, X.; Sun, Z.; Zheng, Y. Nanocomposites of Poly(l-lactide) and Surface-grafted TiO_2 Nanoparticles: Synthesis and Characterization. *Eur. Polym. J.* **2008**, *44*, 2476−2481.

(27) Torres, F. G.; Nazhat, S. N.; Fadzullah, S. H.; Maquet, V.; Boccaccini, A. R. Mechanical Properties and Bioactivity of Porous PLGA/TiO_2 Nanoparticle-filled Composites for Tissue Engineering Scaffolds. *Compos. Sci. Technol.* **2007**, *67*, 1139−1147.

(28) Diez-Pascual, A. M.; Diez-Vicente, A. L. Effect of TiO_2 Nanoparticles on the Performance of Polyphenylsulfone Biomaterial for Orthopaedic Implants. *J. Mater. Chem. B* **2014**, *2*, 7502−7514.

(29) Diez-Pascual, A. M.; Diez-Vicente, A. L. High-Performance Aminated Poly(phenylene sulphide)/ZnO Nanocomposites for Medical Applications. *ACS Appl. Mater. Interfaces* **2014**, *6*, 10132−10145.

(30) Diez-Pascual, A. M.; Diez-Vicente, A. L. ZnO-reinforced Poly(3-hydroxybutyrate-co-3-hydroxyvalerate) Bionanocomposites with Antimicrobial Function for Food Packaging. *ACS Appl. Mater. Interfaces* **2014**, *6*, 9822−9834.

(31) Colthup, N. B.; Day, L. H.; Wiberley, S. E. *Introduction to Infrared and Raman Spectroscopy,* 3rd ed.; Academic Press, Inc: San Diego, CA, 1990.

(32) Nyquist, R. A.; Kagel, R. O. *Infrared Spectra of Inorganic Compounds;* Academic Press, Inc.: New York, 1971; p 214.

(33) Diez-Pascual, A. M.; Martínez, G.; Gómez, M. A. Synthesis and Characterization of Poly(ether ether ketone) Derivatives Obtained by Carbonyl Reduction. *Macromolecules* **2009**, *42*, 6885−6892.

(34) Zhang, Y.; Yuan, S.; Zhou, W.; Xu, J.; Li, Y. Spectroscopic Evidence and Molecular Simulation Investigation of the $\pi−\pi$ Interaction between Pyrene Molecules and Carbon Nanotubes. *J. Nanosci. Nanotechnol* **2007**, *7*, 2366−2375.

(35) Patel, P.; Hull, T. R.; McCabe, R. W.; Flath, D.; Grasmeder, J.; Percy, M. Mechanism of Thermal Decomposition of Poly(Ether Ether Ketone) (PEEK) From a Review of Decomposition Studies. *Polym. Deg. Stab.* **2010**, *95*, 709−718.

(36) Alexander, L. E.; Krieger, R. E. *X-ray Diffraction Methods in Polymer Science;* Wiley: New York, 1969.

(37) Diez-Pascual, A. M.; Naffakh, M.; González-Domínguez, J. M.; Ansón, A.; Martínez-Rubi, Y.; Martínez, M. T.; Simard, B.; Gomez, M. A. High Performance PEEK/Carbon Nanotube Composites Compatibilized with Polysulfones- I. Structure and Thermal Properties. *Carbon* **2010**, *48*, 3485−3499.

(38) Ramani, R.; Alam, S. Composition Optimization of PEEK/PEI Blend using Model-free Kinetics Analysis. *Thermochim. Acta* **2010**, *511*, 179−188.

(39) Vankrevelen, D. W.; Hoftyzer, P. J. *Properties of Polymers;* Elsevier Scientific: New York, 1976.

(40) Diez-Pascual, A. M.; Diez-Vicente, A. L. Poly(3-hydroxybutyrate)/ZnO Bionanocomposites with Improved Mechanical, Barrier and Antibacterial Properties. *Int. J. Mol. Sci.* **2014**, *15*, 10950−10973.

(41) Goodwin, A. A.; Simon, G. P. Dynamic Mechanical Relaxation Behaviour of Poly(ether ether ketone)/Poly(ether imide) Blends. *Polymer* **1997**, *38*, 2363−2370.

(42) Fox, T. G. Influence of Diluent and of Copolymer Composition on the Glass Temperature of a Polymer System. *Bull. Am. Phys. Soc.* **1956**, *1*, 123.

(43) Massey, L. K. *The Effect of Sterilization Methods on Plastics and Elastomers,* 2nd ed.; William Andrew, Inc.: New York, 2005.

(44) Amini, A. M.; Wallace, J. S.; Nukavarapu, S. P. Short-Term and Long-Term Effects of Orthopedic Biodegradable Implants. *J. Long-Term Eff. Med. Implants* **2011**, *21*, 93−122.

(45) Williams, D. F. In *Implants in Surgery;* Williams, D. F., Roaf, R., Maisels, D. O., Eds.; W. B. Saunders Company: Philadelphia, PA, 1973; p 173.

(46) Bhimaraj, P.; Burris, D.; Sawyer, W. G.; Toney, G.; Siegel, R. W.; Schadler, L. S. Tribological Investigation of the Effects of Particle Size, Loading and Crystallinity on Poly(ethylene) Terephthalate Nanocomposites. *Wear* **2008**, *264*, 632−637.

(47) Unal, H.; Mimaroglu, A. Comparison of Tribological Performance of PEEK, UHMWPE, Glass Fiber Reinforced PTFE and PTFE and PTFE Reinforced PEI Composite Materials under Dry and Lubricated Conditions. *J. Polym. Eng.* **2012**, *32*, 349−354.

(48) Friedrich, K.; Schlarb, A. K. In *Tribology of Polymeric Nanocomposites,* Briscoe, B. J., Ed.; Tribology and Interface Enginnering Series 55; Elsevier: Oxford, U.K., 2008.

(49) Zhong, Y. J.; Xie, G. Y.; Sui, G. X.; Yang, R. Poly (ether ether ketone) Composites Reinforced by Short Carbon Fibers and Zirconium Dioxide Nanoparticles: Mechanical Properties and Sliding Wear Behavior with Water Lubrication. *J. Appl. Polym. Sci.* **2011**, *119*, 1711−1720.

(50) Lakes, R. S.; Katz, J. L. Dielectric Relaxation in Cortical Bone. *J. Appl. Phys.* **1977**, *48*, 808−811.

(51) Albertin, K. F.; Valle, M. A.; Pereyra, I. Study of MOS Capacitors with TiO_2 and SiO_2/ TiO_2 Dielectric Gate. *J. Integr. Circuits Syst.* **2007**, *2*, 89−93.

(52) Noori, F. T. M.; Alajaj, E. A.; Al-Nasrawy, D. K. A.C Conductivity and Dielectric Properties of Epoxy - TiO_2 Nanocomposites. *Iraqi J. Phys.* **2011**, *9*, 102−108.

(53) Wu, J.-Y.; Li, C.-W.; Tsai, C.-H.; Chou, C.-W.; Chen, D.-R.; Wang, G.-J. Synthesis of Antibacterial TiO_2/PLGA Composite Biofilms. *Nanomed. Nanotechnol.* **2014**, *10*, 1097−1107.

(54) Neal, A. L. What can be Inferred from Bacterium-Nanoparticle Interactions about the Potential Consequences of Environmental Exposure to Nanoparticles? *Ecotoxicology* **2008**, *17*, 362−371.

(55) Cabeen, M. T.; Jacobs-Wagner, C. Bacterial Cell Shape. *Nat. Rev. Microbiol.* **2005**, *3*, 601−610.

(56) Dalai, S.; Pakrashi, S.; Chakravarty, S.; Hussain, S.; Chandrasekaran, N.; Mukherjee, A. Studies on Interfacial Interactions of TiO_2 Nanoparticles with Bacterial Cells under Light and Dark Conditions. *Bull. Mater. Sci.* **2014**, *37*, 371−381.

(57) Sayes, C. M.; Wahi, R.; Kurian, P. A.; Liu, Y.; West, J. L.; Ausman, K. D.; Warheit, D. B.; Colvin, V. L. Correlating Nanoscale Titania Structure with Toxicity: a Cytotoxicity and Inflammatory Response Study with Human Dermal Fibroblasts and Human Lung Epithelial Cells. *Toxicol. Sci.* **2006**, *92*, 174−185.